

# Dynamic Modeling of the 4 DoF BioRob Series Elastic Robot Arm for Simulation and Control

Thomas Lens, Jürgen Kunz, and Oskar von Stryk

Simulation, Systems Optimization and Robotics Group, Technische Universität  
Darmstadt, Hochschulstraße 10, 64289 Darmstadt, Germany  
{lens,stryk}@sim.tu-darmstadt.de  
www.sim.tu-darmstadt.de, www.biorob.de

**Abstract.** This paper presents the modeling of the light-weight BioRob robot arm with series elastic actuation for simulation and controller design. We describe the kinematic coupling introduced by the cable actuation and the robot arm dynamics including the elastic actuator and motor and gear model. We show how the inverse dynamics model derived from these equations can be used as a basis for a position tracking controller that is able to sufficiently damp the oscillations caused by the high, nonlinear joint elasticity. We present results from simulation and briefly describe the implementation for a real world application.

**Keywords:** flexible joint robot, modeling, control, biologically inspired robotics, series elastic actuation

## 1 Introduction

Elasticity in the actuation of robotic arms was for a long time seen as undesirable. When introducing a series elasticity in the joint actuation, reduced torque and force bandwidth and increased controller complexity for oscillation damping and tracking control are the result. Research on series elastic actuators [13] however, showed that mechanical compliance in the joint actuation can simplify force control in constrained situations, increase safety because of the low-pass filtering of torque and force peaks between the decoupled joint and gearbox, and increase performance of specific tasks because of the possibility to store mechanical energy in the elasticity. For example, the increase of performance for throwing was examined in [18]. In [19], an actuation approach with two motors per joint increasing torque bandwidth without compromising safety was examined. A classification of elastic joint actuation principles is given in [17].

Flexible link manipulators are also subject to current research. But these systems are even harder to control, especially when dealing with multiple degrees of freedom, and do not introduce significant advantages compared to joint elasticity. An overview over research on flexible joint and link systems with an emphasis on flexible links is given in [6].

The modeling of an elastic joint robot with a reduced model was presented in [14]. The complete model and analysis of the model structure was derived in [15],

and complemented by [7]. The control of elastic joint robots with a controller relying solely on motor-based sensor data was presented in [16]. The use of full state feedback was examined in [1] and [5]. Feedforward/feedback control laws are covered in [3]. A good overview over modeling and control methods for robot arms with joint and link flexibility is given in [4].

## 2 BioRob Arm Design

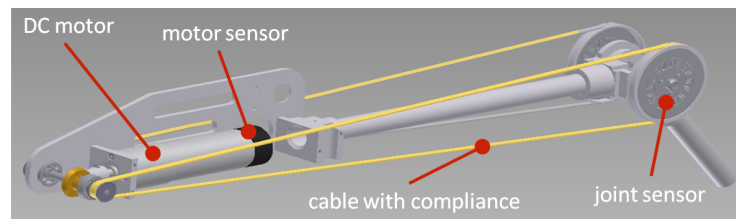


**Fig. 1.** BioRob robot arm actuation principle.

In this work, the BioRob arm, an equilibrium-controlled stiffness manipulator, is analyzed. The mechanical design of this robot arm is depicted in Figure 1. The arm consists of a very lightweight structure with rigid links, elastically actuated by DC motors driving the joints by pulleys and cables with built-in mechanical compliances. Alternative actuation concepts such as pneumatic muscles [8] exhibit inherent compliance and omit the need for gearboxes, but are slower, have a restricted range of operation and are suited for mobile applications only to a very limited extent. Electrical motors on the other hand are robust, allow high speeds, exhibit excellent controllability and are well suited for highly mobile applications. The construction and actuation principle is described in more detail in [11,9].

The general properties of series elasticity in the actuation were described in Section 1. The specific properties of the BioRob arm concept compared to other series elastic concepts are reduced link mass and inertia (a total mass of 4 kg), reduced power consumption, and a significantly lower joint stiffness (ranging between 4 and 20 Nm), in total resulting in increased safety for applications with direct human-robot interaction. As a downside, the use of cable and pulley actuation increases friction and the series elasticity with particularly low joint stiffness demands special efforts regarding oscillation damping. Therefore, an appropriate controller structure is needed.

## 3 Kinematics Model

The BioRob robot arm consists of four elastically actuated joints. To model the kinematics of the robot arm, it is sufficient to model the rigid link structure,

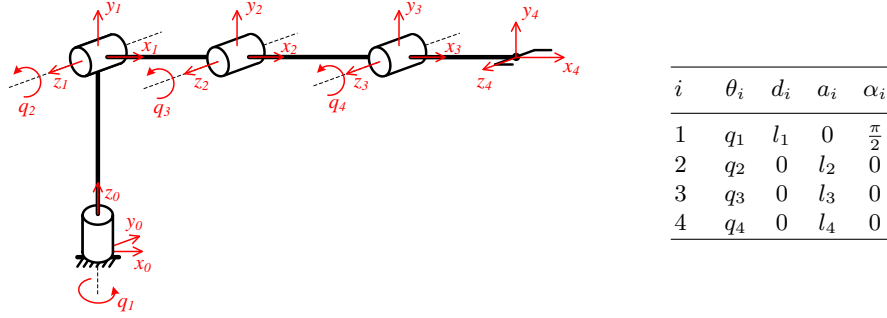


Fig. 2. BioRob 4 DOF robot arm kinematic structure and table with DH parameters.

because the joint elasticity has no effect on kinematics when using joint sensors. Link elasticity is negligible for loads not exceeding the nominal load. Thus, the same modeling methods as used for rigid link robots without elasticity in the actuation can be used, as can be seen in picture 2, where the DH-parameters are listed. As mentioned above, the kinematics model depends only on the joint angular positions  $q_i$  and not on the motor angular positions  $\theta_i$ .

Especially for control, the equilibrium positions of the joints are important. These are the joint positions  $q_i$  and motor positions  $\theta_i$  where the elasticity between motor and joint produces no torque. Normally, the equilibrium position of the joints corresponds to the current position of the motors. This is not the case, however, if the motor is mounted neither on the link it actuates nor on the previous link. Then an additional deflecting pulley becomes necessary. As depicted in Figure 3, the motor driving joint four is fixed to link two and coupled with a deflection pulley (radius  $r_{d3}$ ) in joint three to joint four. Because of the kinematic coupling between link four and three, the equilibrium position of this motor not only depends on  $q_4$ , but also on  $q_3$ , because the cable wraps around the guiding pulley. The amount of cable that wraps around the pulley on joint three is equal to the amount of cable that unwinds from the pulley driving joint four:

$$r_{d3} q_3 = -r_4 \Delta q_4 \quad \Rightarrow \quad \Delta q_4 = -\frac{r_{d3}}{r_4} q_3 . \quad (1)$$

This correction term has to be considered when calculating the equilibrium positions. The resulting joint equilibrium position vector of the manipulator for given angular motor positions  $\boldsymbol{\theta}$  and joint positions  $\boldsymbol{q}$  is:

$$\hat{\boldsymbol{q}}(\boldsymbol{\theta}, \boldsymbol{q}) = \begin{pmatrix} \theta_1 \\ \theta_2 \\ \theta_3 \\ \theta_4 - \frac{r_{d3}}{r_4} \cdot q_3 \end{pmatrix} = \boldsymbol{\theta} - \boldsymbol{\alpha}_c(\boldsymbol{q}) . \quad (2)$$

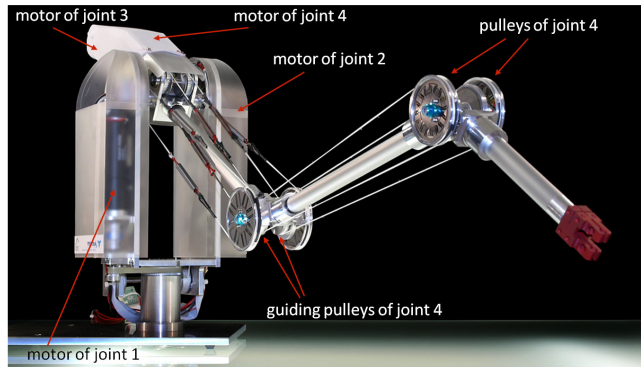


Fig. 3. Position of motors on the BioRob arm.

## 4 Dynamics Model

The dynamics model is used for simulation and controller design. In simulation, the behavior of the model can be studied without the need to perform time-consuming experiments, also avoiding wear of the hardware. It is especially useful for examining scenarios such as collision detection, which are difficult to perform with the hardware. In simulation, it is also possible to provide additional data, that would be difficult to measure, such as collision reaction forces.

However, only effects can be studied that are modeled with sufficient accuracy. The most important effects are the robot arm dynamics consisting of the dynamics of the rigid structure and the joint elasticity, described in Section 4.2. The dynamics model of the motors (Section 4.1) is required to be able take actuator saturation into account. It also allows to simulate the torque loads and peaks caused by collisions.

The primary requirement for the dynamics model is steady state accuracy, which is important for the controller design. Besides the steady state equations and parameters of motors and robot arm, the nonlinear joint elasticity is to be modeled accurately, shown in Section 4.2, due to the low elasticity and therefore large spring deflection. The second important requirement is the accurate modeling of the joint oscillations caused by the joint elasticity. An accurate model of this behavior allows for a better controller design in simulation.

### 4.1 Motor Model

Motors can be controlled to deliver a desired torque  $\tau_m$  which can be seen as the input of the system. Instead of using the simple torque source model, a more complete model of the electrical motor dynamics allows for the examination of the motor currents and voltages, which are bounded in reality. The motors used in the BioRob robot arm are DC motors. The effect of the armature inductance can be neglected compared to the other dynamics of the motor. The electrical

dynamics can be described as:

$$u = R_a i + k_v \cdot \dot{\theta} = \frac{R_a}{k_t} \tau_m + k_v \cdot \dot{\theta} \quad (3)$$

with input voltage  $u$ , armature resistance  $R_a$ , torque constant  $k_t$ , speed constant  $k_v$  and generated motor torque  $\tau_m$ , which drives the rotor. The mechanical dynamics of a freely rotating motor are:

$$I_m \ddot{\theta} + d_m \dot{\theta} = \tau_m . \quad (4)$$

When connected to the robot, the mechanical motor model has to be modeled together with the robot arm mechanics to receive the mechanical dynamics equations of the coupled system. This is described in the following section.

In most cases, electrical motors require gearboxes to achieve the desired torques. These can be modeled with a transmission ratio  $z$  reducing the speed  $\dot{\theta}$  of the motor:

$$\dot{\theta}^* = \frac{1}{z} \dot{\theta} \quad \text{with} \quad |z| > 1 , \quad (5)$$

which increases the torque  $\tau_m$  of the motor. The gearbox also introduces additional friction  $d_g$  and inertia  $I_g$ . For a compact model representation, all motor variables and parameters will be used with respect to the joint side, as *reflected variables*:

$$\tau_m^* = z \cdot \tau_m - d_g \cdot \dot{\theta}^* \quad (6)$$

$$I_m^* = z^2 \cdot I_m + I_g \quad (7)$$

$$d_m^* = z^2 \cdot d_m + d_g . \quad (8)$$

All variables marked with an asterisk are reflected variables calculated with respect to the joint. Further on, only these will be used and for the sake of simplicity, they will not be asterisked.

## 4.2 Robot Arm Dynamics

The model of a BioRob joint as shown in Figure 4 can be transformed into a model of a series elastically actuated joint shown in Figure 5. This is possible if the mass of the cables and elastic parts is so small that the kinetic energy of these elements can be neglected compared to the kinetic energy of the other mechanical robot arm parts. In this case, the transformation can be performed by adapting some of the model parameters. The mass of the motor can be added to the link it is fixed to and the transmission ratios of the gearbox and the cable and pulley elements can be multiplied. All variables can then be calculated as reflected variables with respect to the joint side, as described in the former section.

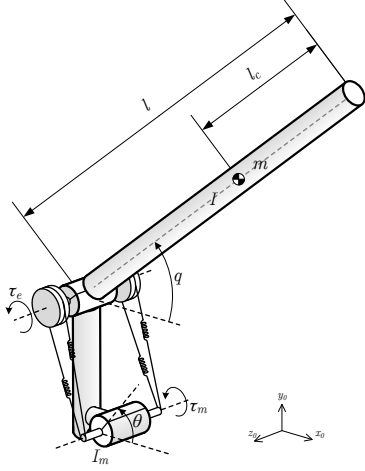


**Fig. 4.** Single joint of the BioRob arm.

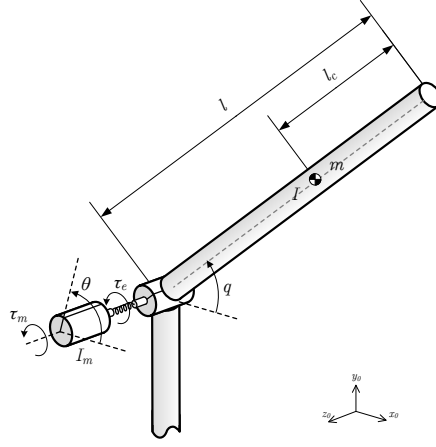


**Fig. 5.** Joint actuated by a Series Elastic Actuator.

The nonlinear joint spring characteristics curve is a function of the deviation of the joint position  $q_i$  of its equilibrium position  $\hat{q}_i$ , which is normally the motor position  $\theta_i$ , but can also be dependent of the position of previous joints, as described in Section 3:

$$\tau_e = k_e(\hat{q} - q). \quad (9)$$

Figure 6 shows the spring characteristic of the fourth joint. The joint elasticity of each joint was chosen according to the expected maximum load torque.

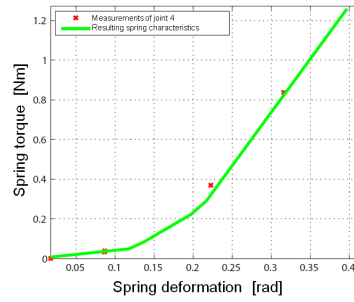


**Fig. 6.** Nonlinear spring characteristic of joint 4.

The multibody dynamics of the robot arm and the motors can be described by using the reduced model of elastic joint robots. For formal derivation of these

equations see [14,16]:

$$\mathbf{M}(\mathbf{q})\ddot{\mathbf{q}} + \mathbf{C}(\mathbf{q}, \dot{\mathbf{q}})\dot{\mathbf{q}} + \mathbf{D}\dot{\mathbf{q}} + \mathbf{g}(\mathbf{q}) = \boldsymbol{\tau}_e \quad (10)$$

$$\mathbf{I}_m\ddot{\boldsymbol{\theta}} + \mathbf{D}_m\dot{\boldsymbol{\theta}} + \boldsymbol{\tau}_e = \boldsymbol{\tau}_m \quad (11)$$

Equation (10) describes the dynamics of the rigid structure with mass matrix  $\mathbf{M}$ , Coriolis matrix  $\mathbf{C}$ , gravity torque vector  $\mathbf{g}$ , and diagonal friction matrix  $\mathbf{D}$ . Equation (11) describes the dynamics of the motor rotors with the diagonal motor rotor inertia matrix  $\mathbf{I}_m$ , diagonal friction matrix  $\mathbf{D}_m$  and motor torque  $\boldsymbol{\tau}_m$ . The mass matrix consist of the inertia and mass of the links, including the motor masses, which are added to the links where they are mounted (see Figure 3). The mass of the cables and mechanical elasticity is negligible. The diagonal matrix  $\mathbf{I}_m$  consists of the motor rotor inertias  $I_{m_{i_{zz}}}$  with respect to the rotor rotating axis. These are the reflected motor inertia values as stated in Section 4.1.

Because the motors are mounted on the first and second joint and therefore moving with low kinetic energy, and because of the large reduction ratios (overall reduction ratios  $z_i$  between 100 and 150), it is possible to neglect the effects of the inertial couplings between the motors and the links, so that the reduced model can be used, as stated in [14]. Otherwise, a more general model would have to be used [15]. Also, the fact that the motors are not located in the joints but mounted on the links, would have to be considered and modeled [12].

## 5 Inverse Model for Tracking Control

### 5.1 Inverse Model

For sufficiently high (but still finite) joint stiffness  $K_e$ , a singular perturbation model can be used [10]. It consist of a slow subsystem, given by the link dynamics equations, and a fast subsystem describing the elasticity. It can be used as a basis for composite control schemes. The joint stiffness of the BioRob manipulator, however, is too low for this approach. Instead, an inverse model is used for the control law [3].

The calculation of computed torque for a given trajectory  $\mathbf{q}_d(t)$  is more difficult with elastic joints, because the desired motor trajectories  $\boldsymbol{\theta}_d(t)$  are not known. With the desired link trajectory we calculate the link equilibrium positions from the joint elasticity equation (9):

$$\hat{\mathbf{q}}_d = \mathbf{k}_e^{-1}(\boldsymbol{\tau}_{e,d}) + \mathbf{q}_d \quad (12)$$

Applying the rigid link dynamics (10) and transforming the equilibrium positions in motor positions with (2) yields the desired motor trajectory that produces the given desired joint trajectory  $\mathbf{q}_d(t)$ :

$$\boldsymbol{\theta}_d = \mathbf{k}_e^{-1} \left( \mathbf{M}(\mathbf{q}_d)\ddot{\mathbf{q}}_d + \mathbf{C}(\mathbf{q}_d, \dot{\mathbf{q}}_d)\dot{\mathbf{q}}_d + \mathbf{D}\dot{\mathbf{q}}_d + \mathbf{g}(\mathbf{q}_d) \right) + \mathbf{q}_d + \boldsymbol{\alpha}_c(\mathbf{q}_d) \quad (13)$$

The desired motor torques  $\tau_{m,d}$  can then be calculated through Equation (11):

$$\tau_{m,d} = \mathbf{I}_m \ddot{\boldsymbol{\theta}}_d + \mathbf{D}_m \dot{\boldsymbol{\theta}}_d + \boldsymbol{\tau}_{e,d}, \quad (14)$$

requiring the second derivative of (13), however. Feedforward laws for the linear joint elasticity case were presented in [3]. This approach would demand a linearization of Equation (6), which would be inaccurate. Therefore, the desired motor trajectory is used for control instead of the desired motor torque.

## 5.2 Control

The desired link trajectory  $\mathbf{q}_d$  and the desired motor trajectory  $\boldsymbol{\theta}_d$  (13) can be used for a controller as shown in Figure 7. Each elastic joint can be described by an ordinary differential equation of order four, which is the length of the complete state vector. The BioRob arm sensor system measures motor  $\theta_i$  and joint  $q_i$  positions, so that following state variables are chosen:  $(q \ \dot{q} \ \theta \ \dot{\theta})$ . This representation has the advantage that only the first derivative is needed, which can be obtained by numerical differentiation.

A simplified control structure can be obtained when using only the steady state torque in (13):

$$\boldsymbol{\theta}_d = \mathbf{k}_e^{-1}(\mathbf{g}(\mathbf{q}_d)) + \mathbf{q}_d + \boldsymbol{\alpha}_c(\mathbf{q}_d). \quad (15)$$

This controller structure uses a global nonlinear calculation of the motor set-point, which linearizes each joint around the current desired position, assuming a sufficiently accurate model. Each joint can then be controlled by a linear controller for all states to receive damped and exact steady state behavior.

In addition to the controller, we also use an approximation of a global gravitational compensation  $\mathbf{g}(\mathbf{q})$ , which is exact in steady state. We assume a motor with controlled torque output (3).

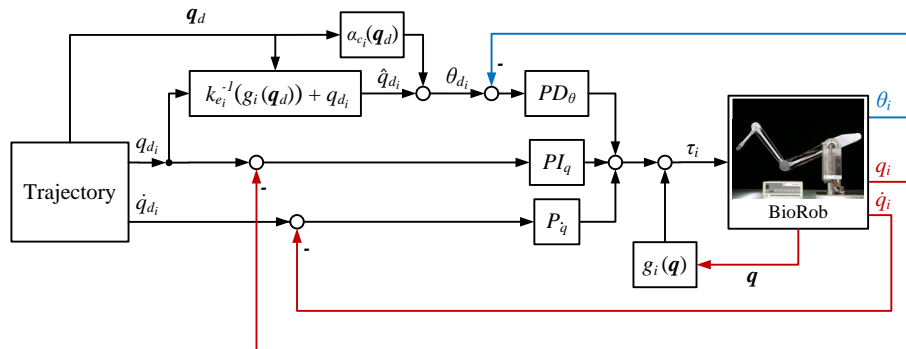
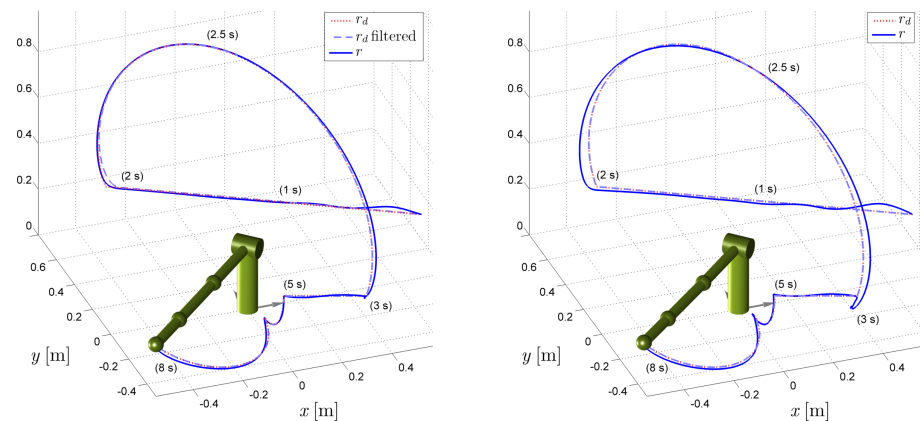


Fig. 7. Control structure for joint  $i$ .

## 6 Simulation Experiments

For the evaluation of the presented controller, a simulation model consisting of the models presented in the former chapters was implemented. The values of the model parameters were obtained by identification and optimization with measurements of the real hardware. The joint stiffness ranges from 4 to 20 Nm/rad, the motors are limited to 10 Nm.

The trajectory used for evaluation of the controller is oriented toward a typical application (Figure 10), but also consists of segments of linear motion in Cartesian space. The desired joint trajectories  $\mathbf{q}_d$  were piecewise generated by cubic interpolation of joint trajectories calculated by inverse kinematics. These trajectories were then low pass filtered. Figure 8 shows the increased performance when using slight filtering with two time constants. As can be seen, critical trajectory points are smoothed ( $t = 2$  s), whereas stationary points are preserved ( $t = 3$  s).



(a) Low pass filtering of the joint trajectory with time constants  $T_1 = T_2 = 0.05$  s.

(b) Without trajectory filtering.

**Fig. 8.** Effect of the joint trajectory low pass filtering.

Figure 9 shows how the joint sensor information is used for damping the oscillations caused by the joint elasticity. As can be seen in Figure 9(a), good steady state accuracy can be obtained with an accurate steady state model even if no joint information is available.

To evaluate the robustness of the controller design with respect to modeling errors and external disturbances, model parameters of the simulation model were altered (Fig. 11(a)) and external forces (Fig. 11(b)) were applied to the robot arm. The additional weight on the end effector effectively doubles its weight. The controller is not able to prevent overshoot at high accelerations, as can be

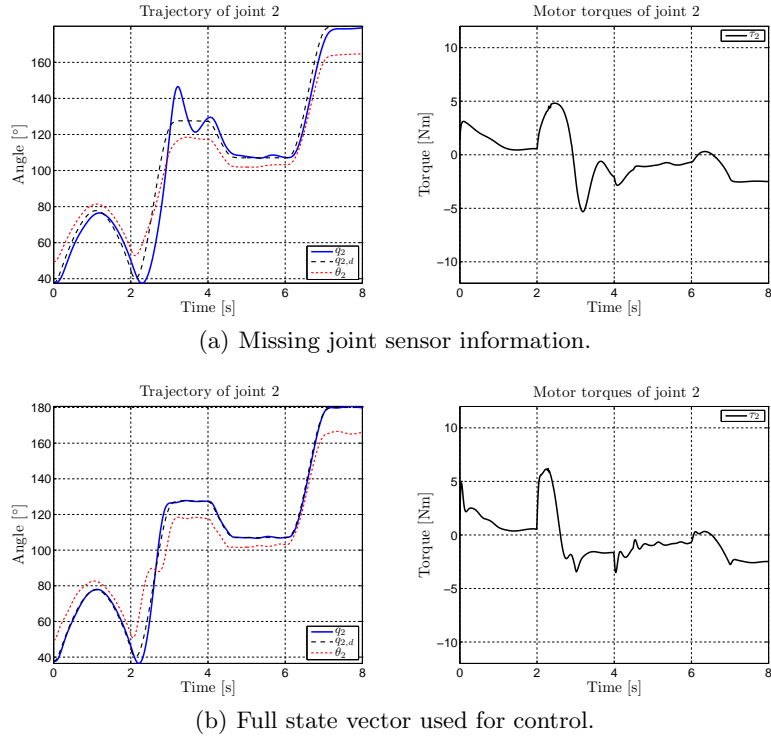


**Fig. 9.** Comparison of the performance of the full state feedback controller and a reduced controller only using motor sensor information.

seen at  $t = 3$  s, but the overall performance is still good and robust. This is also the case for external disturbing forces.

For videos of the implementation of the pick and place application (Figure 10) with the BioRob arm see [2].

## 7 Discussion

The presented controller is based on the steady state model. The remaining dynamics are seen as disturbances on joint level, which are compensated for by a linear full state feedback controller. This design limits the end effector loads and acceleration. With high end effector loads and at high accelerations, the controller is not able to completely damp the oscillations caused by the joint elasticity. The main advantages of the approach are low requirements on the accuracy of the dynamics model parameters. The steady state parameters that are used can be identified with substantial lower effort and higher accuracy than the dynamics parameters.

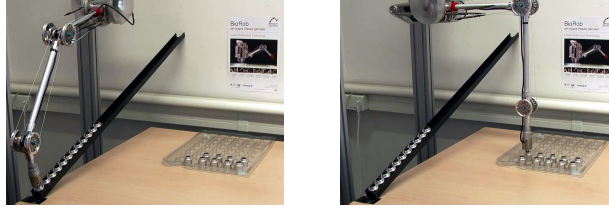
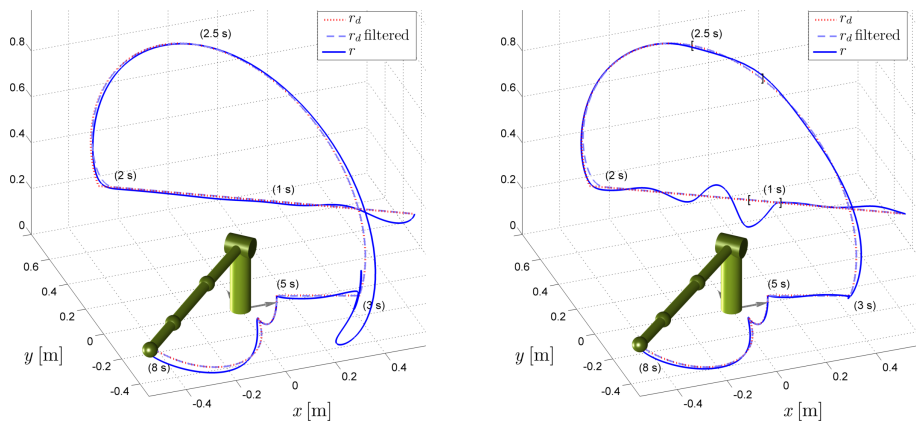


Fig. 10. Pick and place application with the BioRob robot arm [2].



(a) Parameter changes: fourth link weight (doubled), joint and motor friction (doubled).

(b) External forces (marked with square brackets): 5 Nm applied on the second joint from 0.9 to 1.1s and the on first joint from 2.5 to 2.6s.

Fig. 11. Effect of modeling errors and disturbances.

## 8 Conclusion and Outlook

This paper presented the kinematics and dynamics models and a position tracking control scheme for a series elastic joint robot arm with cable and pulley actuation. We pointed out how the desired motor trajectory can be calculated for a given joint trajectory and how it can be used for damping and tracking control. The performance of the controller design was evaluated in simulation. Future research concentrates on control structures for fast feedforward movements, requiring a model-based extension of the presented controller.

**Acknowledgments.** The research presented in this paper was supported by the German Federal Ministry of Education and Research BMBF under grant 01 RB 0908 A. The authors would like to thank A. Karguth and C. Trommer from TETRA GmbH, Ilmenau, Germany for the hardware design and photographs (Fig. 1 and 3) of the BioRob robot arm.

## References

1. Albu-Schäffer, A., Ott, C., Hirzinger, G.: A unified passivity-based control framework for position, torque and impedance control of flexible joint robots. *International Journal of Robotics Research* 26(1), 23–39 (2007)
2. BioRob project website: <http://www.biorob.de>
3. De Luca, A.: Feedforward/feedback laws for the control of flexible robots. In: *Proc. IEEE Intl. Conf. on Robotics and Automation (ICRA)*. vol. 1, pp. 233–240 (2000)
4. De Luca, A., Book, W.: *Springer Handbook of Robotics*, chap. Robots with Flexible Elements, pp. 287–319. Springer (2008)
5. De Luca, A., Siciliano, B., Zollo, L.: PD control with on-line gravity compensation for robots with elastic joints: Theory and experiments. *Automatica* 41(10), 1809 – 1819 (2005)
6. Dwivedy, S.K., Eberhard, P.: Dynamic analysis of flexible manipulators, a literature review. *Mechanism and Machine Theory* 41(7), 749 – 777 (2006)
7. Höppler, R., Thümmel, M.: Symbolic computation of the inverse dynamics of elastic joint robots. In: *Proc. IEEE Intl. Conf. on Robotics and Automation (ICRA)* (2004)
8. Klute, G.K., Czerniecki, J.M., Hannaford, B.: Artificial muscles: Actuators for biorobotic systems. *International Journal of Robotics Research* 21(4), 295–309 (2002)
9. Lens, T., Kunz, J., Trommer, C., Karguth, A., von Stryk, O.: Biorob-arm: A quickly deployable and intrinsically safe, light-weight robot arm for service robotics applications. In: *Proc. 41st International Symposium on Robotics (ISR) / 6th German Conference on Robotics (ROBOTIK)* (2010)
10. Marino, R., Nicosia, S.: On the feedback control of industrial robots with elastic joints: A singular perturbation approach. *Tech. Rep. R-84.01*, University of Rome (1984)
11. Möhl, B.: Bionic robot arm with compliant actuators. In: *Proc. Sensor Fusion and Decentralized Control in Robotic Systems III (SPIE)*. pp. 82–85 (2000)
12. Murphy, S., Wen, J., Saridis, G.: Simulation and analysis of flexibly jointed manipulators. In: *Proc. 29th IEEE Conf. on Decision and Control*. pp. 545–550 vol.2 (1990)
13. Pratt, G., Williamson, M.: Series elastic actuators. *IEEE/RSJ Intl. Conf. on Intelligent Robots and Systems* 1, 399 (1995)
14. Spong, M.W.: Modeling and control of elastic joint robots. *Journal of Dynamic Systems, Measurement, and Control* 109(4), 310–318 (1987)
15. Tomei, P.: An observer for flexible joint robots. *IEEE Transactions on Automatic Control* 35(6), 739–743 (jun 1990)
16. Tomei, P.: A simple pd controller for robots with elastic joints. *IEEE Transactions on Automatic Control* 36(10), 1208–1213 (Oct 1991)
17. Van Ham, R., Sugar, T., Vanderborght, B., Hollander, K., Lefeber, D.: Compliant actuator designs. *Robotics & Automation Magazine, IEEE* 16(3), 81–94 (sep 2009)
18. Wolf, S., Hirzinger, G.: A new variable stiffness design: Matching requirements of the next robot generation. In: *Proc. IEEE Intl. Conf. on Robotics and Automation (ICRA)*. pp. 1741–1746 (2008)
19. Zinn, M., Khatib, O., Roth, B., Salisbury, J.: A new actuation approach for human-friendly robot design. *International Journal of Robotics Research* 23 (4/5), 379–398 (Apr-May 2004)